

1        **QUANTITATIVE ASSESSMENT OF THE RISK OF AIRBORNE TRANSMISSION OF SARS-**  
2                    **CoV-2 INFECTION: PROSPECTIVE AND RETROSPECTIVE APPLICATIONS**

3

4                                    G. Buonanno<sup>1,2</sup>, L. Morawska<sup>2</sup>, L. Stabile<sup>1,\*</sup>

5

6        <sup>1</sup> Department of Civil and Mechanical Engineering, University of Cassino and Southern Lazio, Cassino, FR,

7                                    Italy

8

9        <sup>2</sup> International Laboratory for Air Quality and Health, Queensland University of Technology, Brisbane, Qld,

10                                  Australia

11

12    **\*Corresponding author:**

13    Luca Stabile

14    Department of Civil and Mechanical Engineering,

15    University of Cassino and Southern Lazio, Cassino, FR, Italy

16    Via G. Di Biasio 43, 03043 Cassino (FR), Italy

17    e-mail: l.stabile@unicas.it

18    **Abstract**

19    Airborne transmission is a recognized pathway of contagion; however, it is rarely quantitatively

20    evaluated. This study presents a novel approach for quantitative assessment of the individual

21    infection risk of susceptible subjects exposed in indoor microenvironments in the presence of an

22    asymptomatic infected SARS-CoV-2 subject. The approach allowed the maximum risk for an

23    exposed healthy subject to be evaluated or, starting from an acceptable risk, the maximum

24 exposure time. We applied the proposed approach to four distinct scenarios for a prospective  
25 assessment, highlighting that, in order to guarantee an acceptable individual risk of  $10^{-3}$  for  
26 exposed subjects in naturally ventilated indoor environments, the exposure time should be  
27 shorter than 20 min. The proposed approach was used for retrospective assessment of  
28 documented outbreaks in a restaurant in Guangzhou (China) and at a choir rehearsal in Mount  
29 Vernon (USA), showing that, in both cases, the high attack rate values can be justified only  
30 assuming the airborne transmission as the main route of contagion. Moreover, we shown that  
31 such outbreaks are not caused by the rare presence of a superspreader, but can be likely  
32 explained by the co-existence of conditions, including emission and exposure parameters, leading  
33 to a highly probable event, which can be defined as a “superspreading event”.

34

35 **Keywords:** SARS-CoV-2 (COVID-19) assessment; virus airborne transmission; indoor; ventilation;  
36 coronavirus.

37

## 38 1. Introduction

39 The airborne transmission of a virus and the consequent contagion risk assessment is a complex  
40 issue that requires multidisciplinary knowledge. It is necessary to understand the characteristics  
41 and mechanisms behind the generation of respiratory microdroplets <sup>1,2</sup>, the survival of viruses in  
42 microdroplets <sup>3</sup>, the transport of microdroplets and human exposure to them <sup>4</sup>, and the airflow  
43 patterns that carry microdroplets in buildings <sup>5</sup>. Expiratory human activities generate virus-  
44 carrying microdroplets that are small enough to remain aloft in air during exhalation, talking, and  
45 coughing <sup>2,6,7</sup>. Atomization occurs in the respiratory tract, and droplets are expelled at high speed  
46 during expiration <sup>8,9</sup>. Toques of liquid originating from different areas of the upper respiratory  
47 tract are drawn out from the surface and broken into droplets of different sizes <sup>10</sup>. The findings of

48 early investigations <sup>11-13</sup> served as a foundation for subsequent studies involving temporal and  
49 spatial visualization methods using high-speed cameras <sup>14</sup>, particle image velocimetry <sup>8</sup> and, above  
50 all, increasingly accurate particle counters <sup>6</sup>, which have facilitated the detailed characterization  
51 and quantitation of droplets expelled during various forms of human respiratory exhalation flows.  
52 The issue of the viral load emitted, however, remained difficult to solve. In the past, backward  
53 calculation was used to estimate the emission of an infected subject based on retrospective  
54 assessments of infectious outbreaks only at the end of an epidemic <sup>15-18</sup>. This led to the definition  
55 of emission values for each virus regardless of the type of respiratory act and the metabolic  
56 activity of the infected subject. Recently, the authors presented an approach to evaluate the viral  
57 load emitted by infected individuals with a view to provide new predictive capacities, not currently  
58 available <sup>19</sup>. This approach, based on the oral viral load and the infectivity of the virus, takes into  
59 account the effect of other parameters such as inhalation rate, type of respiratory activity, and  
60 activity level, to estimate the quanta emission rate. This value provides key information for  
61 engineers and indoor air quality experts to simulate airborne dispersion of diseases in indoor  
62 environments. Indeed, the use of exposure risk models in closed environments <sup>20,21</sup> makes it  
63 possible to estimate contagion starting from the emission values of a contagious subject.  
64 The overall approach of emission and exposure modelling represents an essential tool to be  
65 applied in enclosed spaces, and can support air quality experts and epidemiologists in the  
66 management of indoor environments during an epidemic for both prospective and retrospective  
67 assessments.  
68 In this paper we apply a novel approach that takes into account the characteristics of the emitting  
69 subject, the microenvironment, and the exposed subject to calculate the probability of infection  
70 and the individual risk, for both prospective and retrospective assessments of airborne infectious  
71 transmission of SARS-CoV-2. In the case of prospective assessment, various exposure scenarios in

72 indoor environments were analyzed in order to assess the influence of risk mitigation parameters.  
73 In the case of retrospective assessment, we estimated the probability of infection and the  
74 individual risk of two documented outbreaks.

## 75 **2. Materials and methods**

76 To evaluate both prospective and retrospective assessments of the airborne transmission of SARS-  
77 CoV-2, we used a four-step approach to quantify the probability of infection, i.e. the ratio between  
78 infected cases and the exposed population due to exposure in a microenvironment where a SARS-  
79 CoV-2 infected subject is present. The four steps of the proposed approach are: i) evaluation of  
80 the quanta emission rate; ii) evaluation of the exposure to quanta concentration in the  
81 microenvironment; iii) evaluation of the dose of quanta received by an exposed susceptible  
82 subject; and iv) estimation of the probability of infection on the basis of a dose–response model.  
83 The simulations of the probability of airborne transmission of SARS-CoV-2 were performed  
84 applying a Monte Carlo method <sup>22</sup>. Further they adopted the infection risk assessment typically  
85 implemented to evaluate the transmission dynamics of infectious diseases and to predict the risk  
86 of these diseases to the public <sup>17,20,21</sup>.

87 Once the probability of infection was obtained, an approach to evaluate the individual infection  
88 risk, i.e. a parameter that also takes into account how likely the probability of infection can occur,  
89 was also implemented. Individual risk can be easily compared to an acceptable risk, i.e. a target  
90 reference risk that could be suggested by agencies and regulatory authorities to control the  
91 pandemic. In the following sections, the methodologies adopted to evaluate the probability of  
92 infection based on the four step approach (section 2.1) and the individual infection risk (section  
93 2.2) are described. The application of the proposed approach for prospective and retrospective  
94 assessments is described in sections 2.3 and 2.4.

95 2.1 *Estimation of the probability of infection*

96 2.1.1 *Evaluation of the quanta emission rate: the forward emission approach*

97 Recently, Buonanno et al. <sup>19</sup> proposed a forward emission approach to estimate the quanta  
98 emission rate of an infectious subject on the basis of the viral load in the sputum and the  
99 concentration of droplets expired during different activities. A quantum is defined as the dose of  
100 airborne droplet nuclei required to infect a susceptible person. The quanta emission rate ( $ER_q$ ,  
101 quanta  $h^{-1}$ ) was evaluated as:

102

103 
$$ER_q = c_v \cdot c_i \cdot IR \cdot \int_0^{10\mu m} N_d(D) \cdot dV_d(D) \quad (1)$$

104 where  $c_v$  is the viral load in the sputum (RNA copies  $mL^{-1}$ ),  $c_i$  is a conversion factor defined as the  
105 ratio between one infectious quantum and the infectious dose expressed in viral RNA copies,  $IR$  is  
106 the inhalation rate ( $m^3 h^{-1}$ ),  $N_d$  is the droplet number concentration (part.  $cm^{-3}$ ), and  $V_d(D)$  is the  
107 volume of a single droplet ( $mL$ ) as a function of the droplet diameter ( $D$ ). The number and volume  
108 of the droplets ( $V_d$ ) is determined on the basis of data obtained experimentally by Morawska et al.  
109 (2009)<sup>6</sup>.

110 With reference to the SARS-CoV-2 viral load in the mouth, researchers have recently found  $c_v$   
111 values of up to  $10^{11}$  copies  $mL^{-1}$ , which is also variable in the same patient during the course of the  
112 disease <sup>23-26</sup>. In particular, Rothe et al. <sup>24</sup> reported a case of SARS-CoV-2 infection in which  
113 transmission appears to have occurred during the incubation period in the index patient. A high  
114 viral load of  $10^8$  copies  $mL^{-1}$  was found, confirming that asymptomatic persons are potential  
115 sources of SARS-CoV-2 infection. Furthermore, Pan et al. <sup>23</sup>, in a study on 82 SARS-CoV-2 infected  
116 patients, found  $c_v$  values in the range of  $10^8$ – $10^9$  RNA copies  $mL^{-1}$ , also in the previous days and in  
117 the first days of onset of the disease. Consequently, the concentrations of the viral load in the

118 mouth can reach values of  $10^9$  RNA copies  $\text{mL}^{-1}$  and occasionally up to  $10^{11}$  RNA copies  $\text{mL}^{-1}$  during  
119 the course of the disease.

120 The conversion factor,  $c_i$ , i.e. the ratio between one infectious quantum and the infectious dose  
121 expressed in viral RNA copies, barely represents the probability of a pathogen surviving inside the  
122 host to initiate the infection; thus  $c_i=1$  implicitly assumes that infection will occur for each  
123 pathogen (RNA copy in the case of SARS-CoV-2) received by the exposed people. There are  
124 currently no values available in the scientific literature for  $c_i$  for SARS-CoV-2. Watanabe et al. <sup>27</sup>  
125 estimated the infectious doses of several coronaviruses on the basis of data sets challenging  
126 humans with virus HCoV-229E (known as an agent of human common cold) and animals with  
127 other viruses (e.g. mice with MHV-1, considered as a surrogate of SARS-CoV-1). On the basis of the  
128 orders of magnitude of the infectivity conversion factors for the overall data sets, we assumed a  $c_i$   
129 range between 0.01 and 0.1.

130 The quanta emission rate calculation was performed for four different emission profiles (which are  
131 adopted in the risk evaluations described later) evaluated as a combination of expiratory activities  
132 and activity levels: (i) oral breathing during resting; (ii) oral breathing during heavy activity; (ii)  
133 speaking during light activity; and (iv) singing (or loudly speaking) during light activity.

134 Quanta emission rates were calculated using eq. (1) and applying a Monte Carlo method <sup>22</sup> in order  
135 to take into account for the possible variation of the input data. To this end, probability density  
136 functions characteristics of each parameter were considered. In particular, we considered normal  
137 distributions for: (i) the log-transformed  $c_v$  data (average and standard deviation of  $\log_{10}(c_v)$  equal  
138 to 8 and 0.7  $\log_{10}$  (RNA copies  $\text{mL}^{-1}$ ), respectively); and (ii) the infectious dose  $c_i$  (average and  
139 standard deviation equal to 0.025 and 0.125, respectively). A distribution of quanta emission rates  
140 ( $ER_q$ ), was obtained as a result of application of the Monte Carlo method (Figure 1), i.e. the  
141 probability density function of  $ER_q$  ( $\text{pdf}_q$ ).

### 142 2.1.2 Evaluation of the exposure to quanta concentration

143 The second step in evaluating the probability of infection is evaluation of the quanta  
144 concentration to which a susceptible subject is exposed. The quanta concentration at time  $t$ ,  $n(t)$ ,  
145 in an indoor environment is based on the quanta mass balance proposed by Gammaitoni and  
146 Nucci<sup>20</sup>, and can be evaluated as:

147

$$148 \quad n(t) = \frac{ER_q \cdot I}{IVRR \cdot V} + \left( n_0 - \frac{ER_q \cdot I}{IVRR} \right) \cdot \frac{e^{-IVRR \cdot t}}{V} \quad (\text{quanta m}^{-3}) \quad (2)$$

149 where  $IVRR$  ( $\text{h}^{-1}$ ) represents the infectious virus removal rate in the space investigated,  $n_0$   
150 represents the initial number of quanta in the space,  $I$  is the number of infectious subjects,  $V$  is the  
151 volume of the indoor environment considered, and  $ER_q$  is the quanta emission rate ( $\text{quanta h}^{-1}$ ) for  
152 the specific disease/virus under investigation. The quanta concentration calculation adopted here  
153 is based on the following hypotheses: the quanta emission rate is considered to be constant, the  
154 latent period of the disease is longer than the time scale of the model, and the droplets are  
155 instantaneously and evenly distributed in the room<sup>20</sup>. The infectious virus removal rate is the sum  
156 of three contributions<sup>28</sup>: the air exchange rate (AER) via ventilation, the particle deposition on  
157 surfaces ( $k$ , e.g. via gravitational settling), and the viral inactivation ( $\lambda$ ). The deposition rate was  
158 evaluated as the ratio between the settling velocity of super-micrometric particles [roughly  
159  $1.0 \times 10^{-4} \text{ m s}^{-1}$  as measured by Chatoutsidou and Lazaridis<sup>29</sup>] and the height of the emission  
160 source (1.5 m); thus,  $k$  was  $0.24 \text{ h}^{-1}$ . The viral inactivation was evaluated on the basis of the SARS-  
161 CoV-2 half-life (1.1 h) detected by van Doremalen et al.<sup>3</sup>, thus  $\lambda$  was  $0.63 \text{ h}^{-1}$ .

162 In the exposure scenarios tested with the prospective and retrospective approaches, to take the  
163 variability of the input parameters into account, the indoor quanta concentration  $n(t)$  was  
164 determined through eq. (2), applying a Monte Carlo method that adopted the probability density  
165 functions ( $\text{pdf}_q$ ) characteristic of quanta emission rates ( $ER_q$ ). Since the probability density

166 functions of the log-transformed  $\log_{10}(ER_q)$  for the different expiratory activities resulted in a  
167 normal distribution (Shapiro-Wilk test,  $p < 0.01$ ), the quanta concentration  $n(t)$  was evaluated by  
168 providing a Gaussian distribution of  $\log_{10}(ER_q)$  (average and standard deviation values are is  
169 summarized in the results section; see Table 2) and then applying a back-transformation from  
170  $\log_{10}(ER_q)$  to  $ER_q$ . The relative frequency at which a certain quanta concentration occurred for each  
171 time step of simulation, i.e. the probability density function of the quanta concentration ( $pdf_n$ ),  
172 was also obtained as result of the Monte Carlo simulations.

### 173 2.1.3 Evaluation of the dose of quanta received by an exposed susceptible subject

174 The dose of quanta received by a susceptible subject exposed to a certain quanta concentration,  
175  $n(t)$ , for a certain time interval,  $T$ , can be evaluated by integrating the quanta concentration over  
176 time as:

$$178 \quad D_q = IR \int_0^T n(t) dt \quad (\text{quanta}) \quad (3)$$

179 It can be concluded from Eq. (3) that the dose of quanta received by a susceptible subject is  
180 affected by the inhalation rate ( $IR$ ) and subsequently by their activity level. As an example, for the  
181 same exposure scenario [i.e. identical  $n(t)$  and  $T$ ], the dose of quanta received by subjects  
182 performing at a light activity level ( $IR = 1.38 \text{ m}^3 \text{ h}^{-1}$ ; e.g. slowly walking) is more than double that  
183 received by people just sitting or standing ( $IR = 0.54 \text{ m}^3 \text{ h}^{-1}$ ). For the dose, in the exposure  
184 scenarios described in this paper, the Monte Carlo method was applied to eq. (3) considering the  
185 probability density function of the quanta concentration ( $pdf_n$ ), whereas the  $IR$  was considered as  
186 a constant value; thus, the probability density function of the dose ( $pdf_D$ ) was obtained for each  
187 time step of the simulation.



188 *2.1.4 Evaluation of the probability of infection through a dose–response model*

189 The fourth and final step in evaluating the probability of infection is the adoption of a dose–  
190 response model. Several dose–response models are available in the scientific literature for  
191 assessing the probability of infection of airborne-transmissible pathogens <sup>16,17</sup>, including  
192 deterministic and stochastic models, and threshold and non-threshold models.

193 The best-suited dose–response models for airborne transmission of pathogens are the stochastic  
194 models. In particular, exponential models have been mostly adopted in previous studies because  
195 of their suitability and simplicity <sup>27</sup>. Such models consider the pathogens as discrete bundles (i.e.  
196 quanta) distributed in a medium (e.g. saliva/sputum) in a random manner described by the  
197 Poisson probability distribution. When the medium is aerosolized, the pathogen distribution in the  
198 aerosols, and hence their distribution in the air, also follows the Poisson probability distribution.

199 The complex Poisson summation equations can be simplified in an exponential equation <sup>17,27,30</sup>, i.e.  
200 the exponential dose–response model, which evaluates the probability of infection,  $P_I$  (%), of  
201 susceptible people as:

202

203 
$$P_I = 1 - e^{-D_q} = \frac{C}{S} \quad (\%) \quad (4)$$

204 For a unit dose of quanta ( $D_q = 1$ ), the probability of infection  $P_I$  is equal to 63%, from which  
205 derives the definition of “quantum” as the “amount of infectious material to infect  $1-e^{-1}$  (i.e. 63%)  
206 of the people in an enclosed space” <sup>13,20</sup>.

207 In the exponential dose–response model, the variation of host sensitivity to the pathogen is not  
208 considered. More complex models, such as the Beta-Poisson probability distribution, could take  
209 this factor into account <sup>17,27,30</sup>; nonetheless, in the present paper the differences in the exposed  
210 population in terms of susceptibility to the virus will not be considered.

211 The probability of infection  $P_I$  evaluated in the following exposure scenarios was determined  
212 through eq. (4), also applying a Monte Carlo method. To this end, the probability density functions  
213 of the dose of quanta ( $pdf_D$ ) obtained as a result of the Monte Carlo simulation on  $D_q$  were  
214 considered; thus, a probability density function of  $P_I$  was also obtained ( $pdf_P$ ).  
215 The probability of infection represents the ratio between the number of infection cases (C) and  
216 the number of exposed susceptibles (S). In retrospective analyses of documented outbreaks, the  
217 known C/S ratio is typically defined as the “attack rate”.

## 218 2.2 *The individual infection risk and the basic reproduction number*

219 As stated above, the probability of infection ( $P_I$ ) is the expected number of infection cases in  
220 relation to the number of exposed susceptibles (C/S ratio). However, based on eqs. (2-4), such  
221 probability is strongly influenced by the probability density function of the dose ( $pdf_D$ ), which is  
222 influenced in turn by the probability density function of the quanta concentration ( $pdf_n$ ) and by  
223 the probability density function of the quanta emission rate ( $pdf_q$ ). In other words, for a given  
224 exposure scenario (microenvironment, ventilation, inhalation rate of the exposed subject, etc.) the  
225 probability of infection ( $P_I$ ) can assume different values on the basis of the rate of quanta emitted  
226 by the infected subject: the lower the quanta emission rates, the lower the probability of infection  
227 (since all the other parameters affecting the exposure were considered to be constant values).  
228 Thus, when evaluating the individual risk (R) of an exposed person, we should know both the  
229 probability of infection ( $P_I$ ) and the probability of occurrence of such a  $P_I$  value ( $P_P$ ). The latter is  
230 defined by the probability density function  $pdf_P$ . Since the probability of infection ( $P_I$ ) and the  
231 probability of occurrence  $P_P$  are independent events, the individual infection risk, R, can be  
232 evaluated as the product of the two terms:

233

$$234 \quad R = P_I \cdot P_P \quad (\%) \quad (5)$$

235

236 The probability density function of the individual risk,  $pdf_R$ , can be obtained by multiplying all the  
237 possible  $P_i$  values obtained from the application of the Monte Carlo method to the four-step  
238 approach by the corresponding probability of occurrence. The maximum value of  $R$  in eq. (5), i.e.  
239 the mode of the  $pdf_R$ , is of particular interest because it represents the most probable individual  
240 risk for a healthy subject or, in other words, the highest probability of being infected. In a  
241 conservative application of the proposed approach to estimate and reduce the risk of individuals  
242 being together with an infected individual in an indoor environment, the maximum individual  
243 infection risk must be less than an acceptable risk.

244 The US Environmental Protection Agency (EPA) typically uses a target reference risk range of  $10^{-4}$   
245 to  $10^{-6}$  for carcinogens in drinking water <sup>31</sup>, which is in line with World Health Organization (WHO)  
246 guidelines for drinking water quality, which base guideline values for genotoxic carcinogens on the  
247 upper bound estimate of an excess lifetime cancer risk of  $10^{-5}$  <sup>32</sup>. If the estimated lifetime cancer  
248 risk is lower than  $10^{-6}$ , the risk is considered acceptable, while risks above  $10^{-4}$  are considered  
249 unacceptable <sup>33</sup>.

250 The choice of an acceptable contagion risk for SARS-CoV-2 is difficult and certainly questionable.  
251 However, considering the mortality rate of SARS-CoV-2, this turns out to be an order of magnitude  
252 lower than the corresponding value associated with carcinogenic diseases. For this reason, only for  
253 discussion purposes, the value of  $10^{-3}$  is taken as an acceptable risk reference for SARS-CoV-2.

254 For the purpose of managing an epidemic and keeping the infection under control, it is also  
255 important to estimate the basic reproduction number of the infection,  $R_0$ , which is calculated as  
256 the ratio between the number of susceptible people infected ( $C$ ) and the infected subject ( $I$ ). Thus,  
257  $R_0$  can be easily evaluated by multiplying the infection probability,  $P_i$ , by the number of exposed  
258 susceptible individuals ( $S$ ). To control an epidemic, the  $R_0$  value must be less than 1. Therefore, in

259 addition to estimating an acceptable individual infection risk, it is necessary to specifically verify  
260 that, with the crowding expected within the environment, the corresponding value of  $R_0$  is less  
261 than 1.

### 262 2.3 Scenarios in the prospective assessment

263 The proposed four-step approach was applied to different indoor microenvironments by varying  
264 the main parameters in order to evaluate the effect of the influencing parameters. In particular,  
265 four emission profiles of the infected subject <sup>6</sup> and corresponding profiles of the healthy subjects  
266 exposed were chosen. For the sake of simplicity, the simulations were run assuming that the  
267 susceptible subjects remained in the microenvironment for the same length of time as the  
268 infected subject (i.e. the two subjects enter and leave the environment under test together). Each  
269 indoor environment under investigation was tested for three different values of air exchange rate  
270 (AER). Table 1 presents a detailed summary of the four different indoor exposure scenarios  
271 considered to evaluate the risk of airborne transmission of SARS-CoV-2. Scenario A consists of a  
272 hospital room of 100 m<sup>3</sup> where a resting infected patient emits quanta in the room through oral  
273 breathing, whereas the exposed susceptible subjects consist of a member of the medical staff in a  
274 light exercise activity (scenario A-1) and another patient at rest (scenario A-2). In scenario B, the  
275 infection affects two subjects, both oral breathing during a sports activity in a 300 m<sup>3</sup> gym.  
276 Scenario C concerns two subjects (infected and healthy) in light activity while speaking in a generic  
277 300 m<sup>3</sup> office (bank, post office, supermarket, shop, etc.). Finally, scenario D represents an  
278 infected subject singing or speaking loudly in an 800 m<sup>3</sup> room with healthy subjects listening at a  
279 sedentary activity level.

280 **Table 1** - Description of the exposure scenarios tested in the prospective assessment.

Scenario A	Scenario B	Scenario C	Scenario D
------------	------------	------------	------------

Type of indoor environment	Hospital room	Gym	Public indoor environments (e.g. restaurant, bank)	Conference room or auditorium
Emitting subject	Patient (Resting, oral breathing)	Exercising person (heavy exercise, oral breathing)	Speaking person (light exercise, voiced counting)	Singer or conference loud speaker (light exercise, unmodulated vocalization)
Exposed subject	A-1. Medical staff (light exercise) A-2. Patient (resting)	Exercising person (heavy exercise)	Speaking person (light exercise)	Spectator (sedentary activity)
Volume (m <sup>3</sup> )	100	300	300	800
Ventilation, AER (h <sup>-1</sup> )	<ul style="list-style-type: none"> <li>• Natural ventilation 0.5 h<sup>-1</sup>,</li> <li>• Mechanical ventilation 3 h<sup>-1</sup>,</li> <li>• Mechanical ventilation 10 h<sup>-1</sup></li> </ul>			
Deposition rate, $k$ (h <sup>-1</sup> )	0.24			
Inactivation rate, $\lambda$ (h <sup>-1</sup> )	0.63			

281 2.4 *Retrospective assessments: outbreaks in a restaurant in Guangzhou, China, and at choir*  
 282 *rehearsal in Skagit Valley (USA)*

283 2.4.1 *The outbreak in a restaurant in Guangzhou, China*

284 A possible case of airborne transmission was recently documented by Lu et al.<sup>34</sup>. Here, an index  
 285 case patient traveled from the Chinese epidemic epicenter, Wuhan, on 23 January 2020 and ate  
 286 lunch in a restaurant in Guangzhou, China, with his family on 24 January 2020 (family A, 10 people  
 287 sitting at the same table). Later that day, the index patient experienced onset of fever and cough  
 288 and SARS-CoV-2 infection was diagnosed. On the following days, nine other people were  
 289 diagnosed with SARS-CoV-2 infection: four members from family A's table and five other people at

290 two different tables (families B and C). No other customers seated at other tables or waiters were  
291 infected.

292 The restaurant is a 5-floor building without windows; each floor has its own air ventilation system.

293 The third floor dining area, at which the index patient ate lunch, has a floor area of 145 m<sup>2</sup>, with

294 15 tables arranged with a distance between each table of about 1 m. A total of 91 people (83

295 customers, 8 staff members) were in the room during that lunch. The exposure time was variable

296 for the customers: those seated at tables close to the index patient had exposure times of

297 53 minutes (family B) and 73 minutes (family C). The ventilation and air conditioning situation is

298 reported in Lu et al.<sup>34</sup>. Five fan coil air-conditioning units are installed in the room and there is no

299 outdoor air supply; thus, the ventilation relies only upon infiltration and natural ventilation. The

300 authors performed computational fluid dynamics analyses and tracer gas decay tests to obtain

301 more information about the possible air-flow pathway in the room, and to determine the air

302 exchange rate expected during that lunch. The analyses performed showed that, due to the

303 particular installation and use of the fan coils, the room can be divided into different air-flow

304 zones, with well-mixed conditions. The air-flow zone involving the table at which the index patient

305 sat also included the two tables at which the other five infected people sat; and covered an area

306 of roughly 45 m<sup>3</sup>. The tracer gas decay tests revealed a low air exchange rate (mostly due to the

307 absence of an outdoor air supply) in the range of 0.56–0.77 h<sup>-1</sup>.

308 Therefore, on the basis of the available information, the retrospective assessment was applied to

309 this outbreak case, through eqs. (2) and (3), using the following input data: i) room volume of

310 45 m<sup>3</sup>; ii) documented probability of infection, i.e. attack rate, of 45% (i.e. 5 out of 11 people of

311 families B and C (family A members were excluded as they could easily have been infected through

312 other infection routes); iii) average exposure time of 1 h; iv) speaking at a light activity level for all

313 people (both emitting and exposed subjects), and v) average AER = 0.67 h<sup>-1</sup>.

314 *2.4.2 The outbreak at a choir rehearsal in Skagit (USA)*

315 A further possible case of airborne transmission of SARS-CoV-2 was documented by the USA  
316 media ([www.latimes.com/world-nation/story/2020-03-29/coronavirus-choir-outbreak](http://www.latimes.com/world-nation/story/2020-03-29/coronavirus-choir-outbreak)). This case  
317 was recorded on 10 March, in Mount Vernon (Skagit County, Washington State, USA). In a 810 m<sup>3</sup>  
318 hall, 61 choir members (out of a total of 121 regular members) gathered to rehearse, aware of the  
319 practices for the containment of contagion (frequent hand washing and social distancing). None of  
320 the members that attended had evident symptoms of SARS-CoV-2 infection. There was hand  
321 sanitizer at the front door and members refrained from the usual hugs and handshakes; each  
322 person brought their own sheet music. The event lasted from 6:30 pm to 9:00 pm (about 2.5  
323 hours). Within few days, 33 of the 61 participants (53%) were diagnosed with SARS-CoV-2  
324 infection, at least three were hospitalized, and two died<sup>35</sup>.

325 As pointed out by Hamner et al.<sup>35</sup>, the 2.5-hour singing practice could have provided several  
326 opportunities for droplet and fomite transmission (e.g. members sitting close to one another,  
327 sharing snacks, and stacking chairs at the end of the practice). Nonetheless, the abovementioned  
328 voluntary measures put in place would not support the documented spread of the contagion. On  
329 the contrary, the act of singing, itself, might have contributed to transmission through emission of  
330 aerosols, which is affected by loudness of vocalization<sup>19</sup>. This is even more relevant considering  
331 that attack rate of 53.3% (based on 33 confirmed cases) could represent a conservative estimate,  
332 since other 20 probable cases were mentioned by Hamner et al.<sup>35</sup>.

333 As regard the heating and ventilating system, limited information is available: the Fellowship Hall  
334 is heated by a relatively new commercial forced-air furnace with supply and return air grills  
335 situated high on a single wall. The furnace is installed to have both make-up and combustion air,  
336 but it is not known how much fresh air was provided on that evening. During the entire rehearsal  
337 no exterior doors were open. We applied a retrospective assessment to the case of the Skagit

338 Valley choir through eqs. (2) and (3), using the following input data: i) room volume of  $810 \text{ m}^3$ ; ii)  
339 documented probability of infection, i.e. attack rate, equal to 53%; iii) exposure time of 2.5 h; iv)  
340 singing at a light activity level for all people; and v) natural ventilation with an  $\text{AER} = 0.5 \text{ h}^{-1}$ .

### 341 **3. Results and Discussions**

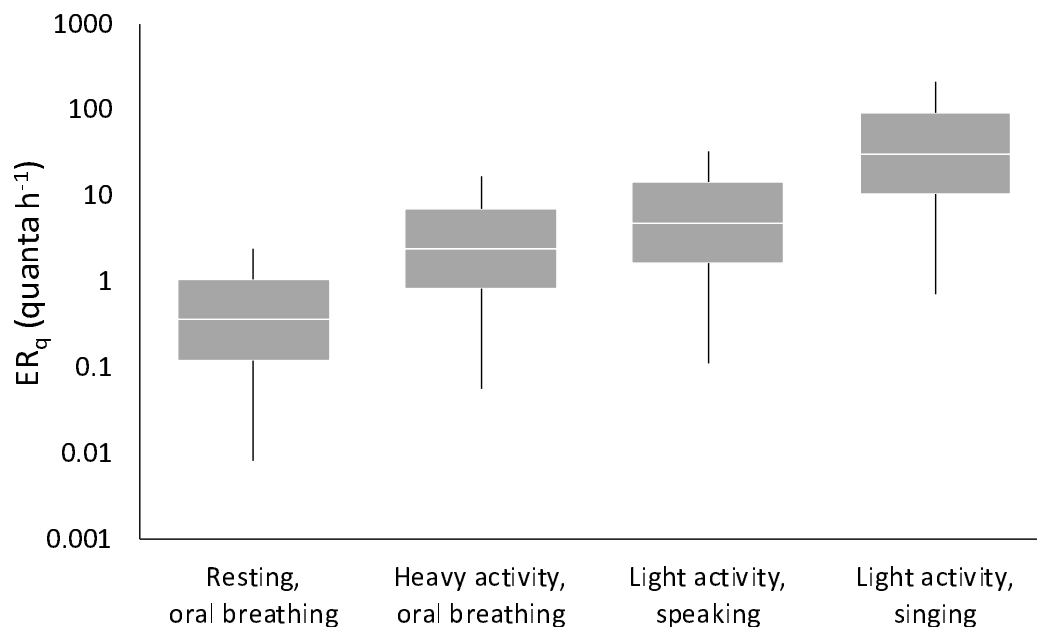
#### 342 *3.1 Statistics of quanta emission rates*

343 Figure 1 and Table 2 show the statistics relating to the quanta emission rates for the four emission  
344 profiles considered in section 2.1. As shown in Buonanno et al.<sup>19</sup>, there are large differences  
345 between the emission profiles. Obviously the lowest values are found under the oral breathing  
346 condition during resting (median value of  $0.36 \text{ quanta h}^{-1}$ ), followed by the oral breathing  
347 condition during heavy activity as the inhalation rate increases ( $2.4 \text{ quanta h}^{-1}$ ), and reaching  $4.9$   
348  $\text{quanta h}^{-1}$  for the increase in aerosol emitted during vocalization<sup>6</sup> and, finally, peaking during  
349 singing/speaking loudly ( $31 \text{ quanta h}^{-1}$ ). Indeed, the rate of particle emission during normal human  
350 speech is positively correlated with the amplitude of vocalization<sup>36</sup>.

351 The probability density functions of the quanta emission rates ( $P_q$ ) were also determined. In  
352 particular, the log-transformed  $\text{ER}_q$  values obtained from the Monte Carlo simulations resulted in a  
353 normal distribution (Shapiro-Wilk test,  $p < 0.01$ ). Table 2 shows the average and standard  
354 deviation values of the  $\log_{10}(\text{ER}_q)$ .

355 We point out that the estimated values present two main uncertainty contributions clearly related  
356 to the limited data currently available for the SARS-CoV-2: i) a still low number of experimental  
357 data for the viral load in the mouth,  $c_v$ , of SARS-CoV-2 infected subjects, ii) unavailable infectivity  
358 conversion factors,  $c_i$ , for SARS-CoV-2; indeed, as mentioned in the methodology section, the  $c_i$   
359 parameter was estimated on the basis of data available for other coronaviruses challenging  
360 humans (only in the case of HCoV-229E) and animals (for all other types of coronavirus).





361

362 **Figure 1** - Statistics of quanta emission rates ( $ER_q$ ) for the four expiratory activities considered in the

363 exposure scenarios. Data reported represent 1<sup>st</sup>, 25<sup>th</sup>, 50<sup>th</sup>, 75<sup>th</sup>, and 99<sup>th</sup> percentiles.

364 **Table 2** -  $ER_q$  (quanta  $h^{-1}$ ) and  $\log(ER_q)$  statistics for SARS-CoV-2 as a function of the expiratory activity and

365 activity level. The log-transformed  $ER_q$  values follow a log-normal distribution; thus, the average and

366 standard deviation values of the  $\log_{10}(ER_q)$  are provided.

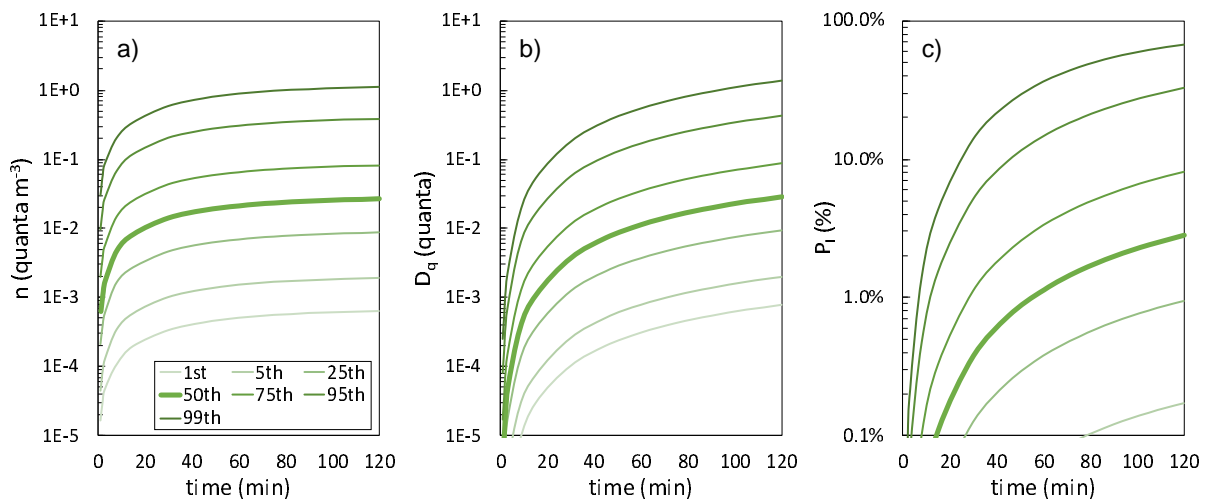
	Resting, oral breathing	Heavy activity, oral breathing	Light activity, speaking	Light activity, singing (or speaking loudly)	
$ER_q$	5 <sup>th</sup> percentile	$2.5 \times 10^{-2}$	$1.7 \times 10^{-1}$	$3.4 \times 10^{-1}$	$2.1 \times 10^0$
	25 <sup>th</sup> percentile	$1.2 \times 10^{-1}$	$8.1 \times 10^{-1}$	$1.6 \times 10^0$	$1.0 \times 10^1$
	50 <sup>th</sup> percentile	$3.6 \times 10^{-1}$	$2.4 \times 10^0$	$4.9 \times 10^0$	$3.1 \times 10^1$
	75 <sup>th</sup> percentile	$1.1 \times 10^0$	$7.2 \times 10^0$	$1.5 \times 10^1$	$9.3 \times 10^1$
	95 <sup>th</sup> percentile	$5.2 \times 10^0$	$3.0 \times 10^1$	$7.1 \times 10^1$	$4.5 \times 10^2$
	99 <sup>th</sup> percentile	$1.6 \times 10^1$	$1.1 \times 10^2$	$2.2 \times 10^2$	$1.4 \times 10^3$
$\log_{10}(ER_q)$	Average	$-4.4 \times 10^{-1}$	$3.9 \times 10^{-1}$	$6.9 \times 10^{-1}$	$1.5 \times 10^0$
	Stand. dev	$7.1 \times 10^{-1}$	$7.1 \times 10^{-1}$	$7.1 \times 10^{-1}$	$7.1 \times 10^{-1}$

367 3.2 Risk management in prospective assessment applications

368 3.2.1 Illustrative example of probability of infection and individual risk evaluation

369 In Figure 2 an illustrative example of quanta concentration  $n(t)$ , dose of quanta ( $D_q$ ), and  
370 probability of infection ( $P_I$ ) trends as a function of time (here shown for 2 h) resulting from the  
371 Monte Carlo simulation for exposure scenario D (singing exhibition, conference speaker) with an  
372 AER =  $0.5 \text{ h}^{-1}$  is shown. In particular, the trends of different percentiles are reported. The example  
373 shows that a person singing/speaking loudly in such a microenvironment can lead to a median  $n(t)$   
374 value after 2 hours equal to  $0.027 \text{ quanta h}^{-1}$  (with a 5<sup>th</sup>–95<sup>th</sup> percentile range of  $<0.002$ –  
375  $0.38 \text{ quanta h}^{-1}$ ). Such concentrations lead to a median dose of quanta received by the subject  
376 exposed for 2 h in a sedentary activity equal to  $0.029 \text{ quanta}$  (with a 5<sup>th</sup>–95<sup>th</sup> percentile range of  
377  $<0.002$ – $0.42 \text{ quanta}$ ), then resulting in a median probability of infection,  $P_I$ , of 2.8% (with a 5<sup>th</sup>–  
378 95<sup>th</sup> percentile range of 0.2%–33.0%). Thus, if higher quanta emission rates are considered, the  
379 indoor quanta concentrations and the consequent probability of infection can be more than 10-  
380 fold the median values.

381



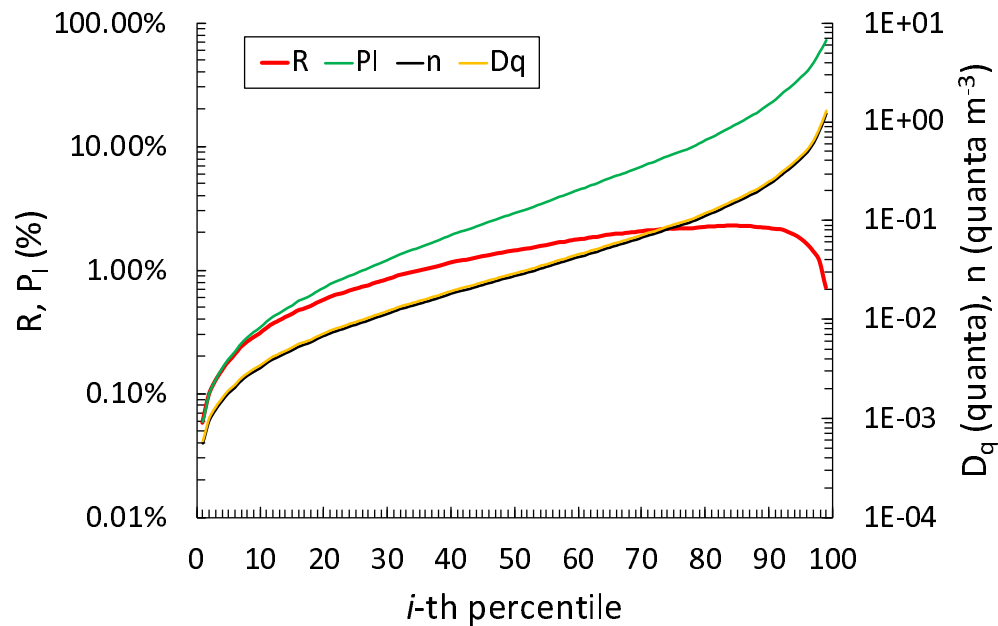
382

383 **Figure 2** - Trends of quanta concentration (a), dose of quanta (b), and probability of infection (c) as a  
384 function of time (here shown for 2 h of exposure) resulting from the Monte Carlo simulation for exposure  
385 scenario D with an AER =  $0.5 \text{ h}^{-1}$ . Different percentiles are reported.

386 In view of the application of a conservative approach that could be essential to reduce the risk of  
387 contagion in indoor environments, using the highest quanta concentration and probability of  
388 infection values can be misleading. Indeed, the probability of occurrence of such high values is  
389 extremely low. Thus, as described in section 2.2, a proper evaluation of the individual infection risk  
390 (R) can be obtained by applying eq. (4), i.e. multiplying the probability of infection ( $P_I$ ) by the  
391 corresponding probability of occurrence ( $P_P$ ). In Figure 3 the probability density functions of  
392 individual infection risk ( $\text{pdf}_R$ ), probability of infection ( $\text{pdf}_P$ ), quanta concentration ( $\text{pdf}_n$ ), and  
393 dose of quanta ( $\text{pdf}_D$ ) after 2 hours of exposure are reported (in terms of R,  $P_I$ , n and  $D_q$  values for  
394 each percentile) for the illustrative example discussed above (i.e. scenario D, AER =  $0.5 \text{ h}^{-1}$ ). The  
395 individual infection risk (R) presents a maximum value ( $R_{\text{max}}$ ) at the 85<sup>th</sup> percentile (2.2%) due to a  
396 probability of infection  $P_I = 14.5\%$  and a probability of occurrence  $P_P = 15\%$ . In other words, the R  
397 value at the 85<sup>th</sup> percentile is the most probable individual infection risk for a healthy susceptible  
398 subject (i.e., the one with the highest chance of occurring). Due to the similarity of the probability  
399 density functions of the four expiration activities resulting from the calculation of the quanta  
400 emission rates ( $\log_{10}(\text{ER}_q)$  reported in Table 2), the  $\text{pdf}_R$  for all the exposure scenarios tested here  
401 was similar to that of the exposure scenario shown in Figure 3 (i.e. the  $R_{\text{max}}$  value occurs in the  
402 narrow range of 84<sup>th</sup>–90<sup>th</sup> percentile).

403 Furthermore, as discussed in section 2.2, the probability density function of the probability of  
404 infection ( $\text{pdf}_P$ ) is mostly influenced by the probability density function of the quanta emission rate  
405 ( $\text{pdf}_q$ ) when moving backwards in the four-step approach; indeed, once the exposure scenario is  
406 defined, all the parameters contributing to the calculation of  $P_I$  (ventilation, room volume, subject

407 activity, etc.) can be considered as constant values. Thus, for a simplified estimate of  $R_{max}$ , the  
408 simplest calculation can be applied (instead of the Monte Carlo method) by just adopting the 85<sup>th</sup>  
409 percentile of the quanta emission rate in the four-step calculation using eqs. (2-4).



410

411 **Figure 3** – Probability density functions of individual infection risk, probability of infection, quanta  
412 concentration, and dose of quanta at  $t = 120$  min for the illustrative example reported in Figure 2 (exposure  
413 scenario A with an air exchange rate of  $0.5\ h^{-1}$ ). The probability density functions are reported as quanta  
414 concentration ( $n$ ), dose of quanta ( $D_q$ ), probability of infection ( $P_I$ ), and individual infection risk ( $R$ ) for each  
415 percentile. The maximum individual infection risk ( $R_{max}$ ) is 1.9% and occurs at the 85<sup>th</sup> percentile  
416 ( $P_I = 14.5\%$ ,  $P_q = 15\%$ ).

### 417 3.2.2 Estimate of the maximum individual risk versus exposure time in indoor environments

418 Figure 4 and Table 3 show the results of the Monte Carlo simulations for the four exposure  
419 scenarios analyzed. The exposure time–risk relationships reported in Figure 4 are essential as they  
420 can be used by choosing either the exposure time or the maximum risk  $R_{max}$  as the independent  
421 variable. In the first case, knowing the exposure time of the healthy subject in the environment in  
422 question, the corresponding individual infection risk can be evaluated and then compared to an

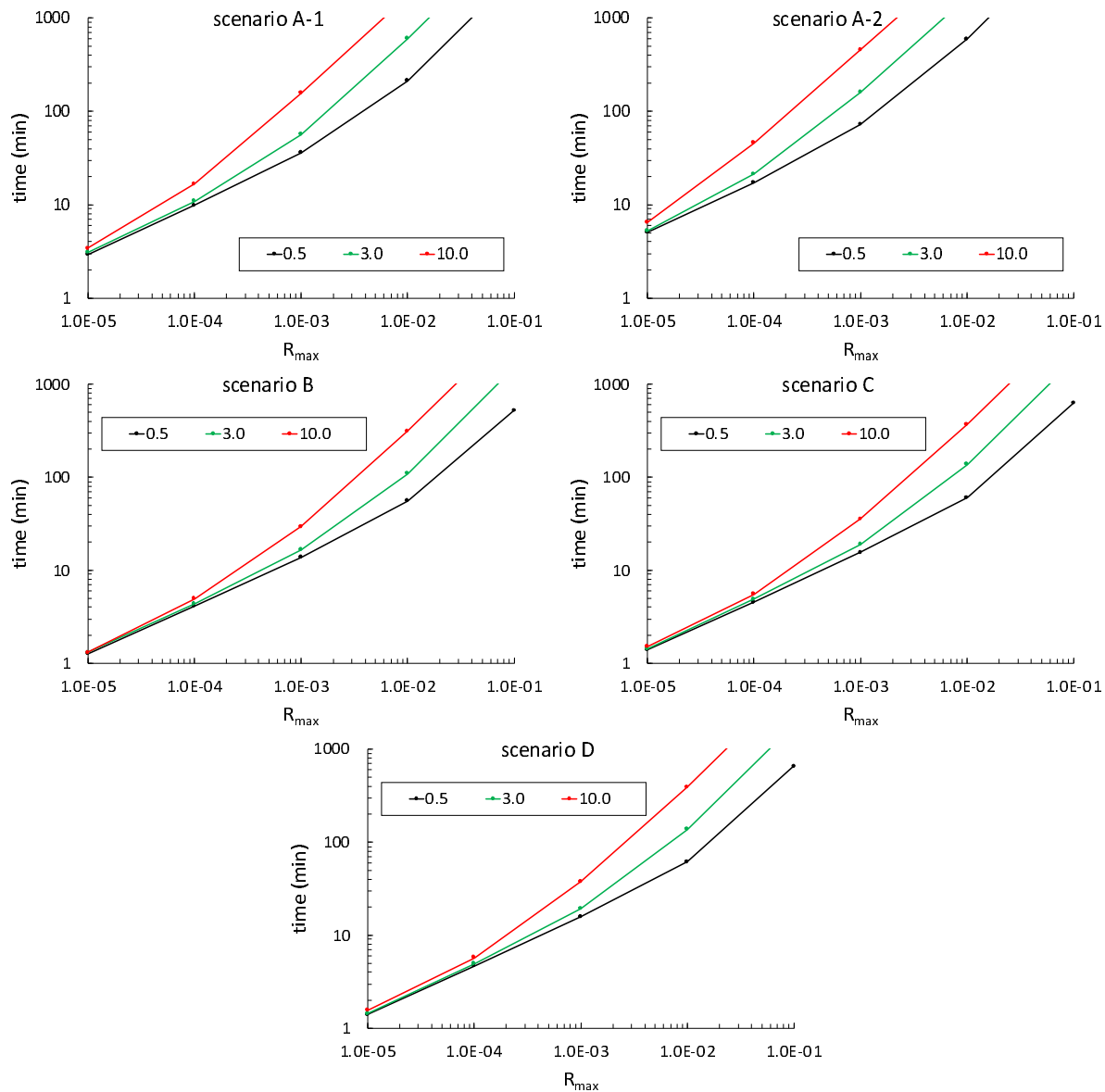
423 acceptable infection risk. In the second case, once an acceptable infection risk has been imposed,  
424 the corresponding maximum exposure time value can be easily assessed. The four scenarios are  
425 examined assuming an acceptable risk value of  $10^{-3}$  as discussed in section 2.3. Since the maximum  
426 value of individual risk occurs roughly at the 90<sup>th</sup> percentile, the corresponding probability of  
427 occurrence of the risk ( $P_P$ ) is 10%; thus, an acceptable individual infection risk of  $10^{-3}$  will roughly  
428 correspond to a probability of infection of  $P_I = 1\%$ . For indoor environments characterized by high  
429 crowding indexes a  $P_I < 1\%$  is essential as it can assure a  $R_0 < 1$  when crowded with up to 100  
430 people. Therefore, assuring an individual infection risk of  $10^{-3}$  also guarantees the control of the  
431 epidemic with an  $R_0 < 1$  for a maximum number of exposed healthy people  $S < 100$ .

432 For the exposure scenario discussed above (scenario D,  $AER = 0.5 \text{ h}^{-1}$ ) the maximum exposure time  
433 to reach an accepted risk of  $R = 10^{-3}$  is very short (16 min); this is due to the high viral load emitted  
434 during singing or speaking loudly leading to high quanta concentrations despite the large volume  
435 available. Obviously, the exposure time can increase with higher ventilation rates, e.g. reaching  
436 38 min in the case of mechanical ventilation at  $10 \text{ h}^{-1}$ . The crowding index of such an indoor  
437 environment ( $800 \text{ m}^3$ ) ranges from  $0.75 \text{ m}^2$  (auditorium) to  $2 \text{ m}^2$  (conference room) per person<sup>37</sup>;  
438 thus, for a room height of 4 m a corresponding floor area of  $200 \text{ m}^2$  will be available, then  
439 resulting in a total number of people simultaneously present in the room ( $S$ ) ranging from 100  
440 (conference room) to 267 (auditorium). Therefore, after 16 min of exposure in the case of natural  
441 ventilation (or 38 min in the case of mechanical ventilation with  $AER = 10 \text{ h}^{-1}$ ), the value of  $R_0$  will  
442 be higher (auditorium) or equal (conference room) to 1. Thus, in the management of the  
443 epidemic, reducing the crowding index could be essential. Accepting higher  $R_{\max}$  values would  
444 clearly increase the maximum exposure time; indeed, in the case of  $R_{\max} = 10^{-2}$ , the exposure time  
445 values would be 62 min and 392 min, for an AER equal to  $0.5 \text{ h}^{-1}$  and  $10 \text{ h}^{-1}$ , respectively. However,

446 in this case, the corresponding value of  $R_0$  would be lower than 1 only for a number of exposed  
447 subjects lower than 10.

448 In scenario C, the infected subject in light activity speaks in a  $300 \text{ m}^3$  environment, along with the  
449 healthy subject. The simultaneous reduction of both the quanta emission rate and the volume  
450 compared to scenario D makes the maximum exposure times for an acceptable infection risk of  $10^{-3}$   
451 comparable to the previous case (15 min and 36 min for ventilation of  $0.5 \text{ h}^{-1}$  and  $10 \text{ h}^{-1}$ ,  
452 respectively). Additionally, in this case, the estimated exposure times would guarantee an  $R_0 < 1$   
453 with  $S < 100$  subjects.

454



455

456 **Figure 4** – Relationship between time of exposure and individual risk ( $R$ ) as a function of the air exchange  
457 rate ( $0.5 h^{-1}$ ,  $3 h^{-1}$ , and  $10 h^{-1}$ ) for the exposure scenarios investigated in the prospective approach and  
458 summarized in Table 1.

459 In scenario A (patient emitting at rest in oral breathing), the maximum exposure time in a hospital  
460 room of  $100 m^3$  for both a medical staff member (scenario A-1) and a patient at rest without  
461 infection (scenario A-2) is evaluated. In both cases the exposure times increase significantly with  
462 the ventilation rate, reaching 36 min and 157 min (scenario A-1), and 72 min and 455 min  
463 (scenario A-2) with AER values of  $0.5 h^{-1}$  and  $10 h^{-1}$ , respectively. However, despite the small size

464 of the room, the  $ER_q$  was extremely small (Table 2); thus, unless a large number of infected  
 465 subjects is simultaneously present in the room, the concentration of viral load in a hospital room  
 466 can be considered low; nonetheless, the overall risk may become relevant due to the long  
 467 exposure times (of 36 and 157 min). Finally, in exposure scenario B (the gym with infected and  
 468 healthy subjects during heavy activity with oral breathing), although there is no vocalization in the  
 469 subject's activity, the high inhalation rate produces considerable  $ER_q$  values, then increasing the  
 470 individual risk; thus, in order to guarantee an acceptable infection risk of  $10^{-3}$  the maximum  
 471 exposure times resulted quite short, i.e. 14 min and 29 min for  $0.5 \text{ h}^{-1}$  and  $10 \text{ h}^{-1}$ , respectively.  
 472 Thus, for all the scenarios investigated, the ventilation conditions strongly influence the risk (or  
 473 the exposure time) of the exposed subject: this difference increases as the accepted risk increases  
 474 as shown in the trends presented in Figure 4. In contrast, if a lower risk was accepted (i.e.  $10^{-4}$  or  
 475  $10^{-5}$ ), increasing the air exchange rate is not leading to the significant reduction of the risk, and  
 476 local exhaust ventilation would be more effective.

477 **Table 3** – Maximum exposure time (min) for the different exposure scenarios to reach an acceptable  
 478 maximum individual infection risk ( $R_{max}$ ).

Exposure scenarios	AER ( $\text{h}^{-1}$ )	Maximum individual infection risk ( $R_{max}$ )				
		$1 \times 10^{-1}$	$1 \times 10^{-2}$	$1 \times 10^{-3}$	$1 \times 10^{-4}$	$1 \times 10^{-5}$
Scenario A-1 - Hospital room	0.5	2797	212	36	10	3
Emitting subject: patient	3.0	7968	600	56	11	3
Exposed subject: Medical staff	10.0	22430	1727	157	17	3
Scenario A-2 - Hospital room	0.5	8039	597	72	17	5
Emitting subject: patient	3.0	21739	1678	159	21	5
Exposed subject: patient	10.0	64333	4671	455	46	6
Scenario B – Gym	0.5	519	55	14	4	1
Emitting subject: Exercising person	3.0	1500	110	16	4	1



Exposed subject: Exercising person	10.0	4119	314	29	5	1
Scenario C – Public indoors	0.5	627	60	15	5	1
Emitting subject: Speaking person	3.0	1812	137	19	5	1
Exposed subject: Speaking person	10.0	4807	372	36	6	1
Scenario D – Conference room	0.5	652	62	16	5	1
Emitting subject: Singer	3.0	1826	138	19	5	1
Exposed subject: Spectator	10.0	5187	392	38	6	2

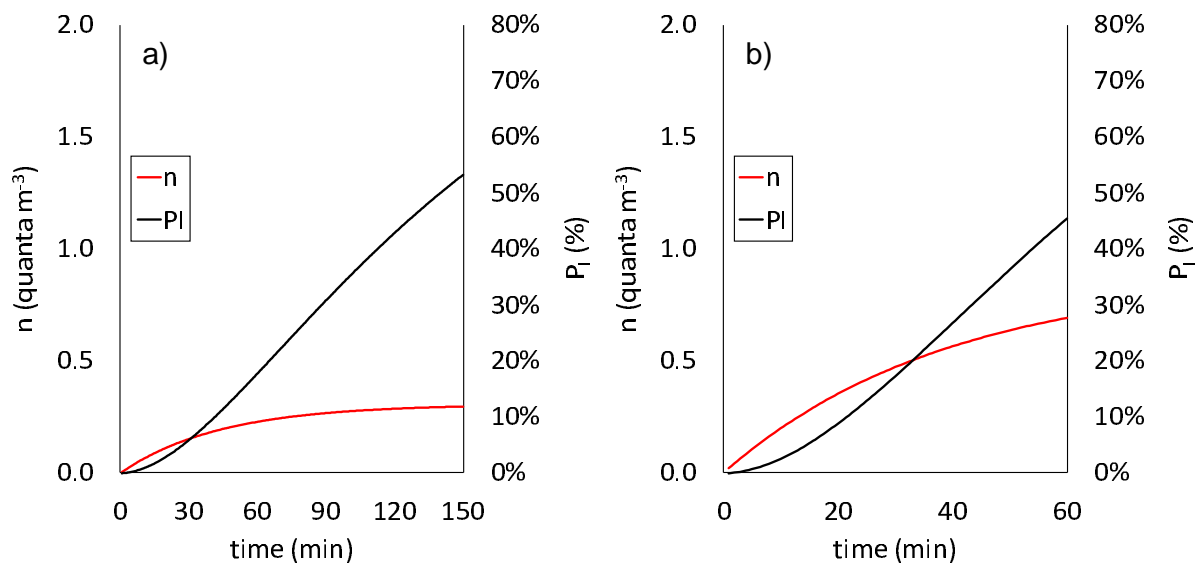
479 3.3 *Retrospective assessment application: the outbreaks in a restaurant in Guangzhou and at a*  
480 *choir rehearsal in Skagit Valley*

481 Figure 5 shows the trends of quanta concentration and probability of infection ( $P_i$ ) evaluated for  
482 the retrospective cases defined in section 2.4 (a restaurant in Guangzhou and the Skagit Valley  
483 choir). The retrospective analysis applied to the restaurant in Guangzhou (Figure 5a) revealed that,  
484 under the boundary conditions considered in the simulation (in terms of room volume, ventilation,  
485 number of exposed people; see section 2.4.1), a probability of infection ( $P_i$ ) after 1 hour of  
486 exposure equal to the attack rate (45%) can be reached for a quanta emission rate of  
487  $ER_q = 61 \text{ quanta h}^{-1}$ . This emission rate, for an emitting subject speaking during light exercise,  
488 occurs at the 93<sup>rd</sup> percentile of the probability density function of  $ER_q$  ( $P_q$ ).

489 Similarly, for the retrospective analysis applied to the Skagit Valley choir (Figure 5b), in order to  
490 reach an attack rate of 53% after 2.5 hours of exposure under the simulation boundary conditions  
491 reported in section 2.4.2, a quanta emission rate of  $341 \text{ quanta h}^{-1}$  is needed. Additionally, in this  
492 case, such an emission rate occurs at the 92<sup>nd</sup> percentile of the probability density function ( $P_q$ ) of  
493 an infected subject while singing.

494 Therefore, for both the analyzed cases in the retrospective analyses, the required  $ER_q$  values to  
495 obtain the documented  $R_e$  fall perfectly within the possible values of the emission profiles under  
496 consideration (i.e. speaking and singing/speaking loudly in light activity reported in Table 2).

497 Moreover, such emission values incur high individual infection risks as they are around the 90<sup>th</sup>  
498 percentile, i.e. at the percentile maximizing the individual infection risk ( $R_{max}$ ). Indeed, the R values  
499 for the restaurant at Guangzhou and the Skagit Valley choir were 3.2% and 3.7%, respectively –  
500 more than one order of magnitude higher than the acceptable risk of  $10^{-3}$ . In these two cases, an  
501 individual risk of  $< 10^{-3}$  would have been obtained with a probability of infection  $P_i = 1.3\text{-}1.4\%$ :  
502 such a  $P_i$  is not actually achievable by varying and optimizing the room ventilation (e.g.  
503  $AER > 100\text{ h}^{-1}$  would be required), and is achievable only by reducing the exposure time of the  
504 susceptible subjects and the quanta emission rates.



505

506 **Figure 5** – Quanta concentration (n) and probability of infection ( $P_i$ ) evaluated for the retrospective cases  
507 applied at the documented outbreaks at (a) the restaurant in Guangzhou and (b) the Skagit Valley choir.

508 To summarize, the retrospective assessment of the two SARS-CoV-2 outbreaks investigated  
509 demonstrate that the documented number of infected people can be explained by means of the  
510 airborne transmission route; indeed, the most probable of the expected events occurred. The  
511 approach and consequent calculation reported here clearly highlights that the explanation of such  
512 a high number of infected people does not necessarily require the presence of a superspreader in  
513 the environment (i.e. an infected person with the highest viral load,  $c_v$ , and infectious dose,  $c_i$ ), but

514 rather a co-existence of conditions, including emission and exposure parameters, leading to a

515 highly probable event, which can be defined as a “superspreading event”.

516

517

## 518 References

- 519 (1) Ai, Z. T.; Melikov, A. K. Airborne Spread of Expiratory Droplet Nuclei between the Occupants of  
520 Indoor Environments: A Review. *Indoor Air* **2018**, *28* (4), 500–524.  
521 <https://doi.org/10.1111/ina.12465>.
- 522 (2) Holmgren, H.; Ljungström, E.; Almstrand, A.-C.; Bake, B.; Olin, A.-C. Size Distribution of Exhaled  
523 Particles in the Range from 0.01 to 2.0 $\mu$ m. *Journal of Aerosol Science* **2010**, *41* (5), 439–446.  
524 <https://doi.org/10.1016/j.jaerosci.2010.02.011>.
- 525 (3) van Doremalen, N.; Bushmaker, T.; Morris, D. H.; Holbrook, M. G.; Gamble, A.; Williamson, B. N.;  
526 Tamin, A.; Harcourt, J. L.; Thornburg, N. J.; Gerber, S. I.; Lloyd-Smith, J. O.; de Wit, E.; Munster, V. J.  
527 Aerosol and Surface Stability of SARS-CoV-2 as Compared with SARS-CoV-1. *N Engl J Med* **2020**.  
528 <https://doi.org/10.1056/NEJMc2004973>.
- 529 (4) Ai, Z. T.; Hashimoto, K.; Melikov, A. K. Airborne Transmission between Room Occupants during  
530 Short-Term Events: Measurement and Evaluation. *Indoor Air* **2019**, *29* (4), 563–576.  
531 <https://doi.org/10.1111/ina.12557>.
- 532 (5) Ai, Z. T.; Huang, T.; Melikov, A. K. Airborne Transmission of Exhaled Droplet Nuclei between  
533 Occupants in a Room with Horizontal Air Distribution. *Building and Environment* **2019**, *163*, 106328.  
534 <https://doi.org/10.1016/j.buildenv.2019.106328>.
- 535 (6) Morawska, L.; Johnson, G. R.; Ristovski, Z. D.; Hargreaves, M.; Mengersen, K.; Corbett, S.; Chao, C. Y.  
536 H.; Li, Y.; Katoshevski, D. Size Distribution and Sites of Origin of Droplets Expelled from the Human  
537 Respiratory Tract during Expiratory Activities. *Journal of Aerosol Science* **2009**, *40* (3), 256–269.  
538 <https://doi.org/10.1016/j.jaerosci.2008.11.002>.
- 539 (7) Morawska, L.; Cao, J. Airborne Transmission of SARS-CoV-2: The World Should Face the Reality.  
540 *Environment International* **2020**, *139*, 105730. <https://doi.org/10.1016/j.envint.2020.105730>.
- 541 (8) Chao, C. Y. H.; Wan, M. P.; Morawska, L.; Johnson, G. R.; Ristovski, Z. D.; Hargreaves, M.; Mengersen,  
542 K.; Corbett, S.; Li, Y.; Xie, X.; Katoshevski, D. Characterization of Expiration Air Jets and Droplet Size

- 543 Distributions Immediately at the Mouth Opening. *Journal of Aerosol Science* **2009**, *40* (2), 122–133.  
544 <https://doi.org/10.1016/j.jaerosci.2008.10.003>.
- 545 (9) Morawska, L. Droplet Fate in Indoor Environments, or Can We Prevent the Spread of Infection?  
546 *Indoor Air* **2006**, *16* (5), 335–347. <https://doi.org/10.1111/j.1600-0668.2006.00432.x>.
- 547 (10) Hickey, A. J.; Mansour, H. M. *Inhalation Aerosols: Physical and Biological Basis for Therapy, Third*  
548 *Edition*; Taylor & Francis Ltd, 2019.
- 549 (11) Duguid, J. P. The Numbers and the Sites of Origin of the Droplets Expelled during Expiratory  
550 Activities. *Edinburgh Medical Journal* **1945**, *LII (II)* (II), 385–401.
- 551 (12) Jennison, M. W. Atomizing of Mouth and Nose Secretions into the Air as Revealed by High Speed  
552 Photography. *Aerobiology* **1942**, *17*, 106–128.
- 553 (13) Wells, W. F. On Airborne Infection: Study II. Droplets and Droplet Nuclei. *American Journal of*  
554 *Epidemiology* **1934**, *20* (3), 611–618. <https://doi.org/10.1093/oxfordjournals.aje.a118097>.
- 555 (14) Tang, J. W.; Noakes, C. J.; Nielsen, P. V.; Eames, I.; Nicolle, A.; Li, Y.; Settles, G. S. Observing and  
556 Quantifying Airflows in the Infection Control of Aerosol- and Airborne-Transmitted Diseases: An  
557 Overview of Approaches. *Journal of Hospital Infection* **2011**, *77* (3), 213–222.  
558 <https://doi.org/10.1016/j.jhin.2010.09.037>.
- 559 (15) Myatt, T. A.; Minegishi, T.; Allen, J. G.; Macintosh, D. L. Control of Asthma Triggers in Indoor Air with  
560 Air Cleaners: A Modeling Analysis. *Environ Health* **2008**, *7*, 43. [https://doi.org/10.1186/1476-069X-7-](https://doi.org/10.1186/1476-069X-7-43)  
561 [43](https://doi.org/10.1186/1476-069X-7-43).
- 562 (16) Rudnick, S. N.; Milton, D. K. Risk of Indoor Airborne Infection Transmission Estimated from Carbon  
563 Dioxide Concentration. *Indoor Air* **2003**, *13* (3), 237–245. [https://doi.org/10.1034/j.1600-](https://doi.org/10.1034/j.1600-0668.2003.00189.x)  
564 [0668.2003.00189.x](https://doi.org/10.1034/j.1600-0668.2003.00189.x).
- 565 (17) Sze To, G. N.; Chao, C. Y. H. Review and Comparison between the Wells–Riley and Dose-Response  
566 Approaches to Risk Assessment of Infectious Respiratory Diseases. *Indoor Air* **2010**, *20* (1), 2–16.  
567 <https://doi.org/10.1111/j.1600-0668.2009.00621.x>.
- 568 (18) Wagner, B. G.; Coburn, B. J.; Blower, S. Calculating the Potential for Within-Flight Transmission of  
569 Influenza A (H1N1). *BMC Medicine* **2009**, *7* (1), 81. <https://doi.org/10.1186/1741-7015-7-81>.

- 570 (19) Buonanno, G.; Stabile, L.; Morawska, L. Estimation of Airborne Viral Emission: Quanta Emission Rate  
571 of SARS-CoV-2 for Infection Risk Assessment. *Environment International* **2020**.  
572 <https://doi.org/10.1101/2020.04.12.20062828>.
- 573 (20) Gammaitoni, L.; Nucci, M. C. Using a Mathematical Model to Evaluate the Efficacy of TB Control  
574 Measures. *Emerging Infectious Diseases* **1997**, 335–342.
- 575 (21) Riley, C.; Murphy, G.; Riley, R. L. Airborne Spread of Measles in a Suburban Elementary School.  
576 *American journal of epidemiology* **1978**, No. 107, 431–432.
- 577 (22) Hammersley, J. M.; Handscomb, D. C. *Monte Carlo Methods*; Chapman and Hall: London & New  
578 York, 1964.
- 579 (23) Pan, Y.; Zang, D.; Yang, P.; Poon, L. M.; Wang, Q. Viral Load of SARS-CoV-2 in Clinical Samples Yang  
580 Pan Daitao Zhang Peng Yang Leo L M Poon Quanyi Wang. *The Lancet* **2020**.
- 581 (24) Rothe, C.; Schunk, M.; Sothmann, P.; Bretzel, G.; Froeschl, G.; Wallrauch, C.; Zimmer, T.; Thiel, V.;  
582 Janke, C.; Guggemos, W.; Seilmaier, M.; Drosten, C.; Vollmar, P.; Zwirgmaier, K.; Zange, S.; Wölfel,  
583 R.; Hoelscher, M. Transmission of 2019-NCov Infection from an Asymptomatic Contact in Germany.  
584 *N Engl J Med* **2020**, 382 (10), 970–971. <https://doi.org/10.1056/NEJMc2001468>.
- 585 (25) To, K. K.-W.; Tsang, O. T.-Y.; Leung, W.-S.; Tam, A. R.; Wu, T.-C.; Lung, D. C.; Yip, C. C.-Y.; Cai, J.-P.;  
586 Chan, J. M.-C.; Chik, T. S.-H.; Lau, D. P.-L.; Choi, C. Y.-C.; Chen, L.-L.; Chan, W.-M.; Chan, K.-H.; Ip, J. D.;  
587 Ng, A. C.-K.; Poon, R. W.-S.; Luo, C.-T.; Cheng, V. C.-C.; Chan, J. F.-W.; Hung, I. F.-N.; Chen, Z.; Chen,  
588 H.; Yuen, K.-Y. Temporal Profiles of Viral Load in Posterior Oropharyngeal Saliva Samples and Serum  
589 Antibody Responses during Infection by SARS-CoV-2: An Observational Cohort Study. *The Lancet*  
590 *Infectious Diseases* **2020**. [https://doi.org/10.1016/S1473-3099\(20\)30196-1](https://doi.org/10.1016/S1473-3099(20)30196-1).
- 591 (26) Woelfel, R.; Corman, V. M.; Guggemos, W.; Seilmaier, M.; Zange, S.; Mueller, M. A.; Niemeyer, D.;  
592 Vollmar, P.; Rothe, C.; Hoelscher, M.; Bleicker, T.; Bruenink, S.; Schneider, J.; Ehmann, R.;  
593 Zwirgmaier, K.; Drosten, C.; Wendtner, C. Clinical Presentation and Virological Assessment of  
594 Hospitalized Cases of Coronavirus Disease 2019 in a Travel-Associated Transmission Cluster. *medRxiv*  
595 **2020**, 2020.03.05.20030502. <https://doi.org/10.1101/2020.03.05.20030502>.

- 596 (27) Watanabe, T.; Bartrand, T. A.; Weir, M. H.; Omura, T.; Haas, C. N. Development of a Dose-Response  
597 Model for SARS Coronavirus. *Risk Anal* **2010**, *30* (7), 1129–1138. <https://doi.org/10.1111/j.1539->  
598 6924.2010.01427.x.
- 599 (28) Yang, W.; Marr, L. C. Dynamics of Airborne Influenza A Viruses Indoors and Dependence on  
600 Humidity. *PLOS ONE* **2011**, *6* (6), e21481. <https://doi.org/10.1371/journal.pone.0021481>.
- 601 (29) Chatoutsidou, S. E.; Lazaridis, M. Assessment of the Impact of Particulate Dry Deposition on Soiling  
602 of Indoor Cultural Heritage Objects Found in Churches and Museums/Libraries. *Journal of Cultural*  
603 *Heritage* **2019**, *39*, 221–228. <https://doi.org/10.1016/j.culher.2019.02.017>.
- 604 (30) Haas, C. N. Estimation of Risk Due to Low Doses of Microorganisms: A Comparison of Alternative  
605 Methodologies. *Am J Epidemiol* **1983**, *118* (4), 573–582.  
606 <https://doi.org/10.1093/oxfordjournals.aje.a113662>.
- 607 (31) Cotruvo, J. A. Drinking Water Standards and Risk Assessment. *Regul Toxicol Pharmacol* **1988**, *8* (3),  
608 288–299. [https://doi.org/10.1016/0273-2300\(88\)90016-5](https://doi.org/10.1016/0273-2300(88)90016-5).
- 609 (32) World Health Organization. *Guidelines for Drinking-Water Quality - 4th Edition*; WHO Regional Office  
610 for Europe, 2011.
- 611 (33) Toner, G. *Innovation, Science, Environment 08/09*; McGill-Queen's University Press, 2008.
- 612 (34) Lu, J.; Gu, J.; Li, K.; Xu, C.; Su, W.; Lai, Z.; Zhou, D.; Yu, C.; Xu, B.; Yang, Z. COVID-19 Outbreak  
613 Associated with Air Conditioning in Restaurant, Guangzhou, China, 2020. *Emerg Infect Dis* **2020**, *26*  
614 (7). <https://doi.org/10.3201/eid2607.200764>.
- 615 (35) Hamner, L.; Dubbel, P.; Capron, I.; Ross, A.; Jordan, A.; Lee, J.; Lynn, J.; Ball, A.; Narwal, S.; Russell, S.;  
616 Patrick, D.; Leibrand, H. High SARS-CoV-2 Attack Rate Following Exposure at a Choir Practice - Skagit  
617 County, Washington, March 2020. *Morbidity and Mortality Weekly Report* **2020**, *69*.
- 618 (36) Asadi, S.; Wexler, A. S.; Cappa, C. D.; Barreda, S.; Bouvier, N. M.; Ristenpart, W. D. Aerosol Emission  
619 and Superemission during Human Speech Increase with Voice Loudness. *Scientific Reports* **2019**, *9*  
620 (1), 2348. <https://doi.org/10.1038/s41598-019-38808-z>.

621 (37) European Committee for Standardisation. UNI EN 15251 - Indoor Environmental Input Parameters  
622 for Design and Assessment of Energy Performance of Buildings Addressing Indoor Air Quality,  
623 Thermal Environment, Lighting and Acoustics. **2008**.  
624